FLUIDIZATION

1. Introduction

Gas–solids fluidization is the levitation of a bed of particles by a gas. Intense solids mixing and good gas–solids contact create an isothermal system having good mass transfer (qv). The gas-fluidized bed is ideal for many chemical reactions, drying (qv), mixing, and heat-transfer applications. Solids can also be fluidized by a liquid or by gas and liquid combined. Liquid and gas–liquid

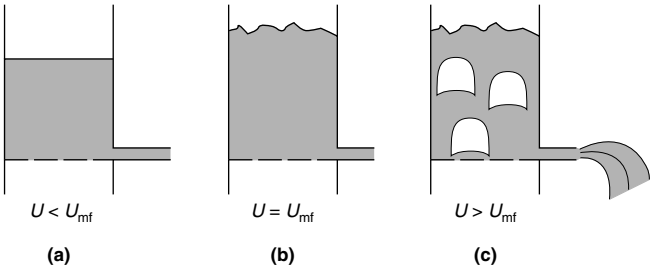

Fig. 1. Fluidized-bed behavior where U is the superficial gas velocity and U_{mf} is the minimum fluidization velocity: (**a**) packed bed, no flow; (**b**) fluid bed, uniform expansion; and (**c**) bubbling fluid bed, flow.

fluidization applications are growing in number, but gas–solids fluidization applications dominate the fluidization field. This article discusses gas–solids fluidization.

The basic concepts of a gas-fluidized bed are illustrated in Figure 1. Gas velocity in fluidized beds is normally expressed as a superficial velocity, U, the gas velocity through the vessel assuming that the vessel is empty. At a low gas velocity, the solids do not move. This constitutes a packed bed. As the gas velocity is increased, the pressure drop increases until the drag plus the buoyancy forces on the particle overcome its weight and any interparticle forces. At

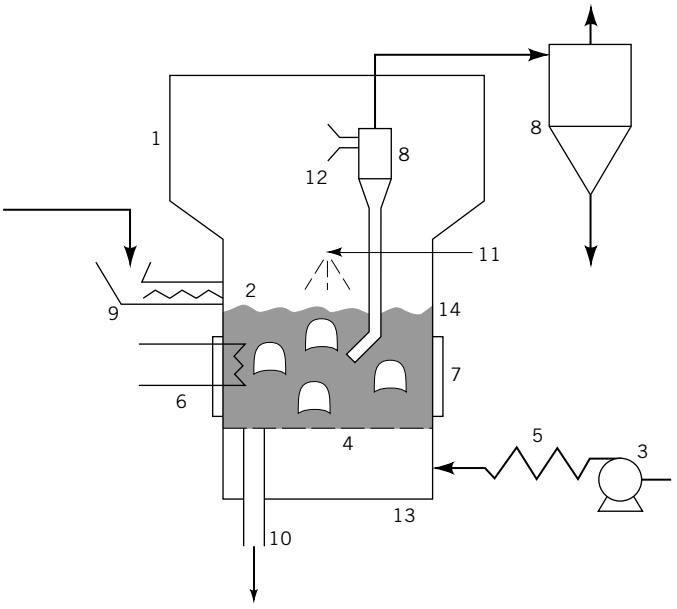

Fig. 2. Multipurpose fluidized bed where 1 represents the shell; 2, solid particles; 3, the blower; 4, the gas distributor; 5, the heat exchanger for fluidizing gas; 6, internal heating or cooling; 7, external heating or cooling; 8, cyclones; 9, the solids feeder; 10, solids offtake; 11, liquid feed; 12, the freeboard; 13, the plenum; and 14, the solids level. Adapted from Ref. 1.

this point, the bed is said to be minimally fluidized, and this gas velocity is termed the minimum fluidization velocity, U_{mf}. The bed expands slightly at this condition, and the particles are free to move about (Fig. 1**b**). As the velocity is increased further, gas voids, or bubbles can form. The solids movement is more vigorous, and the bed expands to accommodate the volume of the bubbles.

Once fluidized, the bed behaves as if it were a fluid. A distinct bed level is maintained and a static pressure head is generated. No flow of solids through a side outlet occurs in a packed bed; however, flow through the opening does occur after a fluidized state has been achieved (Fig. 1**c**).

A generic multipurpose fluidized bed is illustrated in Figure 2 (1). The solids are contained in a vessel and gas is introduced into the system via a distributor, which is typically a drilled plate at the bottom of the vessel. A plenum chamber is provided below the distributor plate. The height of the solids level above the distributor is called the bed height, and the vertical space above the bed height is called the freeboard. A splash zone may exist as a transition between the bed and freeboard. Cyclones, located either in the freeboard or external to the vessel, are used to remove solids from the gas stream. Diplegs can return entrained solids directly to the bed.

2. History of Fluidization and Examples of Applications

Although earlier references dating back to the nineteenth century exist, industrial fluidized-bed applications began with a large-scale Winkler gasifier in 1926. This was the first application of coarse-powder fluidization. Fluidized-bed catalytic cracking (FCC) of crude oil to gasoline was commercialized in 1942, and as of this writing is still the principal application of fine-powder fluidization (2) (see GASOLINE AND OTHER MOTOR FUELS; PETROLEUM). Several catalytic applications, such as acrylonitrile (qv) synthesis, phthalic anhydride manufacture, and Fischer-Tropsch synthesis of fuels from coal-based gas extended the range of catalytic applications following FCC. Spouted beds and moving beds were developed during this same period. Spouted beds process very large particles and are used, for example, in wheat drying and ore roasting (see MINERAL RECOVERY AND PROCESSING; WHEAT AND OTHER CEREAL GRAINS;).

Three-phase biochemical processes were developed in the 1960s as were bubbling bed combustors. In the 1970s, Lurgi commercialized the circulating fluidized bed (CFB) for coarse powders, which operates above the terminal velocity of all the bed particles. The bed inventory in a CFB is continually entrained out of the vessel, recovered, and recirculated. Polyethylene began to be produced in fluidized beds, and this is a principal application of these beds. The 1980s saw commercialization of circulating bed combustion, and production of polypropylene in fluidized beds. Newer areas of application were the production of semiconductor and ceramic materials via chemical vapor deposition in a fluidized bed, and the use of liquid fluidized beds for biological applications (see CERAMICS; ELECTRONIC MATERIALS; ENZYME APPLICATIONS; SEMICONDUCTORS).

Fluidized-bed applications at present may be separated into catalytic reactions, noncatalytic reactions, and physical processes. Examples of fluidized-bed applications include the following:

Chemical Catalytic Processes

Catalytic cracking of heavy petroleum fractions (FCC)
Phthalic anhydride
Acrylonitrile
Aniline (hydrogenation of nitrobenzene)
Synthesis of polyethylene and polypropylene
Fischer-Tropsch synthesis
Oxidation of SO_2 to SO_3
Chlorination or bromination of methane, ethylene, etc
Maleic anhydride (from butane)
Pyridine

Chemical Noncatalytic Processes

Roasting of sulfide and sulfate ores (ZnS, pyrites, Cu_2S, $CuCoS_4$, nickel sulfides)
Calcination (limestones, phosphates, aluminum hydroxide)
Incineration of waste liquids and solids refuse
Coking (thermal cracking)
Combustion of coal and other fuels
Gasification of coal, peat, wood wastes
Carbonization of coal (decomposition without oxygen)
Fluoridation of UO_2 pellets
Catalyst regeneration
Hydrogen reduction of ores
Titanium dioxide

Physical Processes

Drying [eg, phosphates, coal, poly(vinyl chloride) (PVC), polypropylene, foods]
Granulation (eg, pharmaceuticals, fertilizers)
Classification
Blending
Coating (eg, polymer coat on metal object)
High temperature baths
Airslide conveying
Absorption (eg, CS_2)
Filtering of aerosols
Medical beds
Quenching, annealing, tempering

3. Particle Properties

Fluidized-bed design procedures require an understanding of particle properties. The most important properties for fluidization are particle size distribution, particle density, and sphericity.

3.1. Particle Size. The solids in a fluidized bed are never identical in size and follow a particle size distribution. An average particle diameter, d_p, is generally used for design. It is necessary to give relatively more emphasis to the low end of the particle size distribution (fines), which is done by using the surface volume diameter, d_{sv}, to calculate an average particle size:

$$d_{sv} = 1/\Sigma(x_i/d_{pi}) \tag{1}$$

The surface volume diameter is the diameter of a sphere of the same surface area/volume ratio as the actual particle, which is usually not a perfect sphere. The surface volume diameter, which is sometimes referred to as the Sauter mean diameter, is the most useful particle size correlation, because hydrodynamic forces in the fluid bed act on the outside surface of the particle. The surface volume diameter is directly obtained from automated Coulter counters or laser light diffraction devices, which are commonly used to measure particle sizes from 0.5 to 600 μm. X-ray diffraction is commonly used to measure smaller particles (see SIZE MEASUREMENT OF PARTICLES).

Before the advent of light diffraction devices, screen sieving devices or sedimentation methods were commonly used, resulting in the weight-average particle size, d_{pw}. Screen sieving is still used for particles greater than 500 μm in size. A third particle size indicator is the volume average diameter, d_v, which is defined as the diameter of a sphere having the same volume as the particle. For spherical particles, all three particle diameters are nearly equal.

Particle size distribution is usually plotted on a log-probability scale, which allows for quick evaluation of statistical parameters. Many naturally occurring and synthetic powders follow a normal distribution, which gives a straight line when the log of the diameter is plotted against the percent occurrence. However, bimodal or other nonnormal distributions are also encountered in practice.

3.2. Solid Density. Solids can be characterized by three densities: bulk, skeletal, and particle. Bulk density is a measure of the weight of an assemblage of particles divided by the volume the bed occupies. This measurement includes the voids between the particles and the voids within porous particles. The skeletal, or true solid density, is the density of the solid material if it had zero porosity. Fluid-bed calculations generally use the particle density, ρ_p, which is the weight of a single particle divided by its volume, including the pores. If no value for particle density is available, an approximation of the particle density can be obtained by multiplying the bulk density by 2.

3.3. Sphericity. Sphericity, ψ, is a shape factor defined as the ratio of the surface area of a sphere the volume of which is equal to that of the particle, divided by the actual surface area of the particle.

$$\psi = d_{sv}/d_v \tag{2}$$

Rounded materials such as catalyst and round sand have sphericities on the order of 0.9 or higher. Examples of sphericity of various powders are shown in Table 1.

3.4. Angles of Repose and Internal Friction. The angle of repose is the angle that a pile of solids forms with the horizontal plane. The angle of internal friction is the angle with the horizontal that the flow, no-flow boundary forms

Table 1. **Properties of Powders**

Geldart group[a]	Powder	Average particle size, d_p, μm	Particle density, ρ_p, kg/m^3	Angles of: Internal friction, deg	Angles of: Repose, deg	Sphericity, ψ
A	FCC catalyst	60	1400	79	32	0.99
B	sand	500	2000	64	36	0.92
C	ion-exchange resin	30	800	82	29	0.86
D	TCC beads[b]	3000	1000	72	35	1.0

[a] See text.
[b] TCC = Thermofor catalytic cracking.

when solids are flowing over themselves. This angle is a slight function of the solids flow rate. However, a typical angle of internal friction for a nonsticky material without sharp corners generally exceeds 65°. When designing fluidized-bed internal baffles, the baffles generally are angled at greater than 65° to the horizontal to prevent a zone of stagnant solids forming on top.

3.5. Terminal Velocity. The single-particle terminal velocity, U_t, is the gas velocity required to maintain a single particle suspended in an upwardly flowing gas stream. A knowledge of terminal velocity is important in fluidized beds because it relates to how long particles are retained in the system. If the operating superficial gas velocity in the fluidized bed far exceeds the terminal velocity of the bed particles, the particles are quickly removed.

Equations 3–7 indicate the method by which terminal velocity may be calculated. From a hydrodynamic force balance that considers gravity, buoyancy, and drag, but neglects interparticle forces, the single particle terminal velocity is

$$U_t = \left[\frac{4g\, d_p(\rho_p - \rho_g)}{3\rho_g\, C_d}\right]^{1/2} \tag{3}$$

Assuming spherical particles, if the drag coefficient, C_d, is in the laminar regime, the Stokes flow regime then is

$$C_d = \frac{24}{Re_p} \tag{4}$$

where the particle Reynolds number, Re_p, is defined as

$$Re_p = d_p U \rho_g / \mu \tag{5}$$

where μ is the fluid viscosity. The single spherical particle terminal velocity is then

$$U_t = \frac{g\left(\rho_p - \rho_g\right)d_p^2}{18\,\mu} \quad \text{for } Re_p < 0.4 \tag{6}$$

For large particles, C_d is 0.43 and

$$U_t = \left[3.1\left(\rho_p - \rho_g\right) g d_p/\rho_g\right]^{1/2} \quad \text{for } Re_p > 500 \tag{7}$$

These equations indicate that, for small particles, viscosity is the dominant gas property and that for large particles density is more important. All the equations neglect interparticle forces.

The single-particle terminal velocity is only a mathematical limit, because most gas–solids operations operate at a high concentration of solids. Particles interact strongly with each other hydrodynamically, such as by drag reduction owing to shielding and via interparticle forces. The actual slip velocity between particles and gas is then much higher than the single-particle terminal velocity, in many cases tens, or even hundreds of times higher.

In general, the slip velocity, U_{slip}, or the effective terminal velocity for a particle in suspension, U_t^* is

$$U_{\text{slip}} = U_t^* = U_t \cdot f(\epsilon) \tag{8}$$

where f_ϵ is a correction for voidage which accounts for interparticle interactions. The voidage, ϵ, of a fluidized bed is the volume fraction occupied by gas. Many empirical proposals for $f(\epsilon)$ have been made. One of the earliest is the Kozeny-Carman approximation:

$$f(\epsilon) = 0.1\,\frac{\epsilon^2}{(1-\epsilon)} \tag{9}$$

Another approximation, one of the most enduring empirical correlations in multiphase systems, is the Richardson-Zaki correlation for a single particle in a suspension (3):

$$\frac{U}{U_t} = \epsilon^n \tag{10}$$

where n is a function of d_p/D and the Reynolds number and varies from 2.4 to 4.7. The dimensionless plot of particle and gas properties shown in Figure 3 was constructed (4) to cover the entire particle size range. It shows particle properties plotted against gas properties. Voidage, ϵ, is a parameter. The single-particle terminal velocity is determined at $\epsilon = 1.0$, and the minimum fluidization velocity is found at the voidage of loosely packed solids, usually 0.4–0.5.

3.6. Minimum Fluidization Velocity. There is a minimum superficial gas velocity required to just fluidize a bed of solids. The minimum fluidization velocity can be estimated from the Zenz plot (Fig. 3) assuming the voidage at minimum fluidization is 0.5. Alternatively, it can be estimated via a correlation that gives a result equivalent to the plot using a voidage of 0.4. Using both methods defines the range within which a measured value for minimum

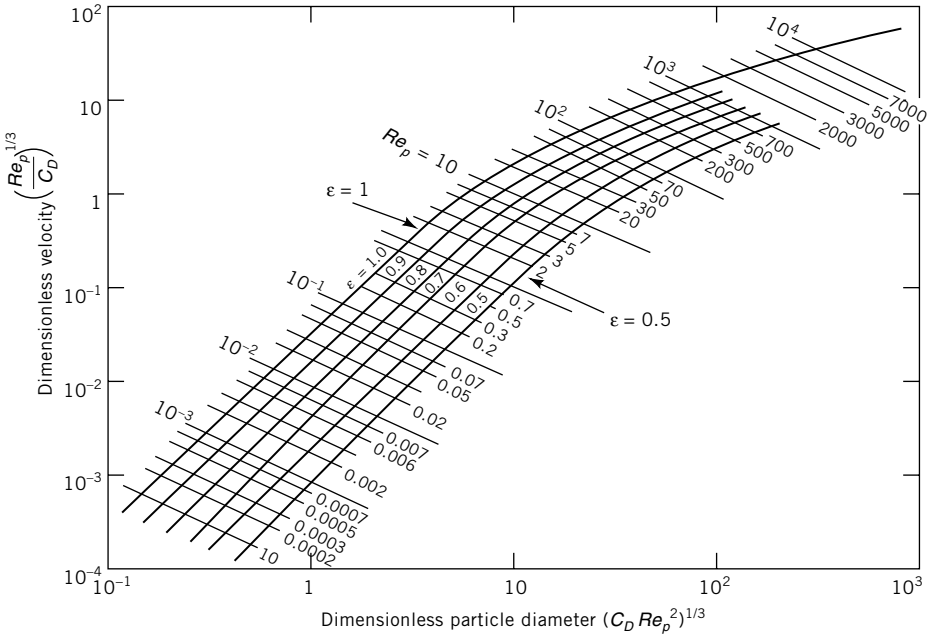

Fig. 3. Zenz plot. Correlation of bed voidage, ϵ, the volume fraction of the fluidized bed that is occupied by gas, for values of ϵ from 1.0 to 0.5, and dimensionless velocity and particle properties, where $C_D = 4gd/_p(\rho_p - \rho_g)/(3\rho_{\ g}U^2)$. The slopingl lines represent the different values of Re_p; $\epsilon = 0.5$ corresponds to the minimum fluidization velocity; $\epsilon = 1$, the terminal velocity. Adapted from Ref. 4.

fluidization velocity falls. The Wen and Yu equation (5), suitable for solids that have a voidage near 0.4, is

$$U_{\mathrm{mf}} = \mu\Big[(1135.7 + 0.0408\,Ar)^{0.5} - 33.7\Big] \Big/ \Big(\rho_g d_p\Big) \tag{11}$$

where the Archimedes number, Ar, is defined as

$$Ar = \rho_g d_p^3 \Big(\rho_p - \rho_g\Big) g/\mu^2 \tag{12}$$

3.7. Particle Regimes. In 1973, particles were classified with respect to how they fluidize in air at ambient conditions into Geldart groups (6) (Fig. 4). Particles that formed bubbles immediately after the gas superficial velocity exceeded U_{mf} were designated as Group B particles. For these particles, the gas velocity at which bubbles first appear in the bed is $U_{\mathrm{mb}} = U_{\mathrm{mf}}$. Group B particles typically have an average particle size from 100 to 700 μm. Dense particles, eg, glass, sand, and ore, are likely to be in Group B. Bubbles in a bed of Group B particles can grow to sizes on the order of a meter in tall, large-diameter beds fluidized at relatively low gas velocities.

Group A particles are smaller or lighter than Group B particles. Most manufactured fluidized-bed catalysts are in the Group A category. Average particle

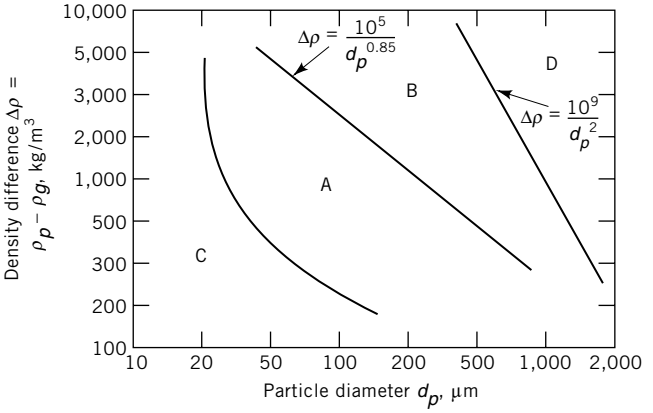

Fig. 4. Geldart group particle classification diagram for air at ambient conditions (6). Group A consists of fine particles; B, coarse particles; C, cohesive, very fine particles; and D, moving and spouted beds.

sizes of catalytic Group A materials range from ~30 to 130 μm. These particles are cohesive owing to interparticle forces and when the gas velocity is increased beyond U_{mf}, the bed continues to expand smoothly without forming bubbles. A velocity is eventually reached when bubbles start to form. Because U_{mb} is > U_{mf}, these particles were designated as Group A for aeratable. The ability to hold aeration enables Group A particles to flow well in transfer pipes in and out of fluidized beds. The small average particle size and the presence of very fine particles promote bubble splitting, and a small maximum stable bubble size can be shown to exist for Group A particles (7).

The maximum bubble size for Group A powders is of great significance for design. The single most important parameter controlling bubble size is particle size distribution, and in particular the <44-μm fines fraction. About 25% fines are optimal for minimal bubble size, and hence for best conversion and highest heat transfer. Industrial processes are normally operated under conditions which suppress bubble formation and growth. The effect of particle size distribution on bubble size for Group A is shown in Figure 5**a**. Increasing the fines fraction decreases bubble size until the bubbles are <25 mm in diameter.

Classical bubbles do not exist in the vigorously bubbling, or turbulent fluidization regimes. Rather, bubbles coalesce constantly, and the bed can be treated as a pseudohomogenous reactor. Small bubble size improves heat transfer and conversion, as shown in Figure 5**b**. Increasing fines levels beyond 30–40% tends to lower heat transfer and conversion as the powder moves into Group C.

Group C particles, smaller and lighter than Group A particles, are designated Group C because they are cohesive. They are usually <30 μm in average particle diameter. The large external surface area and low mass of these particles produce large attractive forces. The particles do not flow well in pipes and are difficult to fluidize. Thus gas flows through the bed in channels called ratholes. When fluid-bed measurements are performed on Group C systems at low gas velocities, a low pressure drop is observed, ie, the gas is flowing in a

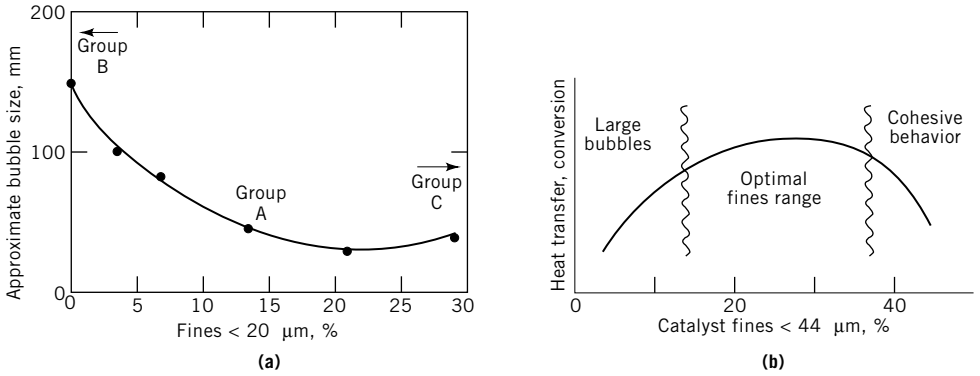

Fig. 5. Effect of fines particle size on (**a**) bubble size for FCC catalyst, of $\rho_P = 1250$ kg/m^3, d_{sv} decreases with increasing fines content, $U = 0.1$ m/s and $D = 0.15$ m (8), and (**b**) on heat transfer and conversion (9,10).

channel without encountering most of the particles. Often, Group C particles can be fluidized by using a high gas velocity to overcome the cohesive forces between the particles, or using fluidization aids such as larger particles, fibrous carbon particles, etc.

Group D particles are large, on the order of 1 or more millimeters (1000 μm) in average particle size. In a fluidized bed, they behave similarly to Group B particles. Because of the high gas velocities required to fluidize Group D particles, it is often more economical to process these particles in spouted or in moving beds, where lower gas rates suffice.

Whereas Geldart's classification relates fluidized-bed behavior to the average particle size in a bed, particle feed sizes may be quite different. For example, in AU: Not listed!fluidized-bed coal (qv) combustion, large coal particles are fed to a bed made up mostly of smaller limestone particles (see COAL CONVERSION PROCESSES).

3.8. Interparticle Forces. Interparticle forces are often neglected in the fluidization literature, although in many cases these forces are stronger than the hydrodynamic ones used in most correlations. The most common interparticle forces encountered in gas fluidized beds are van der Waals, electrostatic, and capillary.

Capillary forces, caused by liquid bridges between the particles, can predominate in applications such as drying, flow out of bins, etc. Electrostatic forces are repulsive forces caused by exchange of electrons between two nonconducting materials, such as sand and a plastic wall. Electrostatic forces are especially significant in cold-flow models and when dry fluidizing gas is used. Capillary forces and electrostatic forces can act on all sizes of particles, large or small.

van der Waals' forces operate between molecules at a very short distance, and hence are significant only for the small, ie, Group C and A, particles. However, these forces can be as important as hydrodynamic forces in many fluidization applications of practical interest. Unlike bubbles, interparticle forces have received little attention, and are usually not included in the basic equations describing fluid bed flow. A noted exception may be found in Ref. 11.

The effect of interparticle forces on the entrainment of Group A powders has been studied (12). When a bed is fluidized at a superficial gas velocity equal to the terminal velocity of the average particle, it takes many hours to entrain the bed because of the interparticle forces holding the particles within. As the gas velocity reaches the terminal velocity of the largest 1% of the particles, it can still take nearly 20 min to empty the bed. These thermodynamic interparticle forces combine with hydrodynamic drag reduction forces so that Group A particles behave as larger clusters of particles. These clusters vary in size from the single particle at low solids concentration to as high as 25 mm for a dense bed (13).

At higher gas velocities, appreciable entrainment of solids starts, but still large clumps of particles fall back along the walls (small tubes) or along the walls and elsewhere (large tubes). This results from clustering of fine powders even in the dilute concentration in the freeboard which is caused by interparticle forces and by drag reduction owing to shielding effects (see POWDERS, HANDLING).

4. Fluidization Regimes

The different fluidized-bed regimes are a function of gas velocity. At a low gas velocity, the solids are in a packed- or fixed-bed state. As the gas velocity is increased, the drag and buoyancy forces eventually overcome the weight of the particles and interparticle forces, and the particles are completely supported by the gas. This is the particulate regime. At minimum fluidization, particles display minimal motion, and the bed is slightly expanded. The bubbling regime, occurs when the gas velocity is increased. Bubbling occurs immediately after minimum fluidization for Group B particles, but there is a gas-velocity range of bubble-free expansion for Group A particles that results from interparticle forces. Poor contacting of gas with solids is a potential problem in the bubbling regime unless bubble size is kept small.

For small columns, growing bubbles can expand to more than one-half of the vessel diameter. When bubbles reach this size, the bed is said to be in the slug flow regime. Bubble size is then limited by the column diameter. Scale-up problems can occur when the ratio of bubble size-to-bed diameter in pilot-scale vessels is greatly exceeded by that ratio in a commercial unit. However, bubble size is kept small in most commercial units by proper choice of particle size distribution and high gas velocities. Gas velocities in the turbulent fluidization regime are high enough for the gas and solids to occupy similar volumes, so that there are no distinct bubbles, just random gas voids. For Group A particles the gas velocity in this regime is above the single-particle terminal velocity of all the particles, and turbulent beds require a system to return the large volumes of entrained solids back to the bed.

To escape bubbling fluidization and move to a circulating bed, the gas velocity is increased further. The fast-fluidization regime is reached where the solids occupy only 5–20% of the bed volume. Gas velocities can easily be 100 times the terminal velocity of the bed particles. Increasing the gas velocity further results in a system so dilute that pneumatic conveying (qv), or dilute-phase transport, occurs. In this regime there is no actual bed in the column.

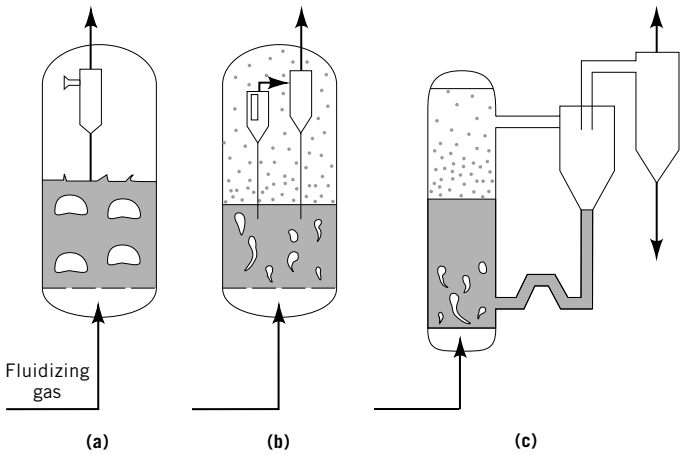

Fig. 6. Schematics of commercially used beds, where the shaded area represents the solids: (**a**) vigorously bubbling, (**b**) turbulent, and (**c**) fast fluidized. Adapted from Ref. 12.

Figure 6 shows how three reactors might appear when operating in the three most common commercial fluidization regimes (12). The vigorously bubbling bed unit (shown with large bubbles, as with Group B particles, or Group A particles which are devoid of <44 μm fines) has a dense bed containing a solids volume fraction typically ranging from 0.5 to 0.35. There is a distinct bed level, and a relatively small amount of solids are entrained with the gas as it leaves the bed. A cyclone is generally used to separate the entrained solids from the gas stream, and this may be either internal, as illustrated in Figure 6**a**, or external to the reactor vessel.

The turbulent fluidized bed has a similar or slightly lower solids volume fraction than the vigorously bubbling bed. There is considerable transport of

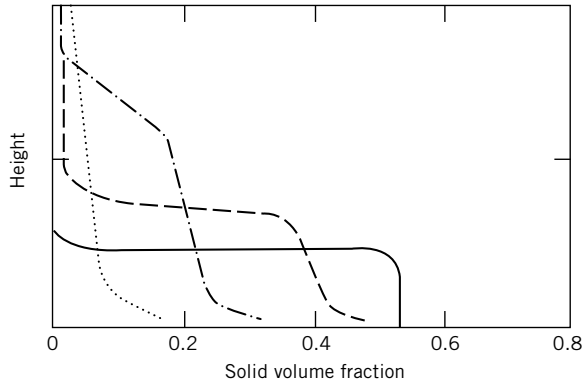

Fig. 7. Axial density profiles in the (—) bubbling, (— — — —) turbulent, and (— · — · —) fast and (·····) riser circulating fluidization regimes. Typical gas velocities for fine particles are 0.1 and 0.5 m/s for the bubbling and turbulent regimes, respectively, and 3 and 10 m/s for the fast and riser circulating beds, respectively.

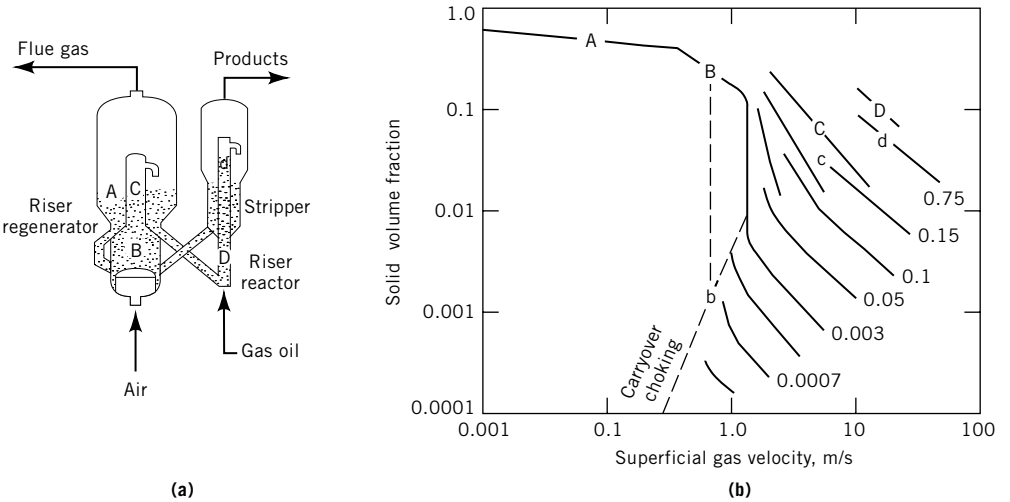

Fig. 8. (**a**) Schematic for an FCC unit showing where the various fluidization regimes are found and (**b**) a corresponding phase diagram for Group A powder (FCC catalyst) where the numbers on the curves represent the superficial solid velocity in m/s. A represents the bubbling regime; B, the turbulent; C, the fast; and D, the riser flow. The lowercase b, c, and d represent solids concentrations near the top of the bed.

solids out of the turbulent bed and the bed level is not very distinct. Large-scale cyclones are needed to return solids to the bed. On average, the bed inventory passes through the cyclones several times per hour.

In the fast-fluidized bed, a distinct bed level does not exist, but there is a long transition zone from the dense turbulent section at the bottom to a dilute regime at the top of the reactor. Large cyclones are needed to collect the large amounts of entrained solids. Fast-fluidized beds are more properly called circulating fluidized beds (CFBs), because the solids are constantly recirculated at high rates around the system. Fast-fluidized beds have the advantages of high through-puts, good mixing, and good gas–solids contact. On the other hand, they are generally more expensive to construct and operate than vigorously bubbling or turbulent fluidized beds. Typical axial density profiles for these fluidization regimes are illustrated in Figure 7.

Many phase diagrams have been proposed to describe fluidization regimes. One such diagram for FCC catalyst, which is the quintessential Group A powder, is shown in Figure 8 (10). Solids volume fraction decreases with increasing gas velocity in the bubbling and turbulent regimes. The density of the dilute transport regime above the turbulent bed is shown via a tie-line B–b. A similar line shows the approximate decrease in axial density between the bottom and the top of a fast bed (C–c) and a more dilute, transported bed, as in FCC riser flow (D–d). As can be seen from the schematic diagram of an FCC riser and regenerator system, all of these regimes can exist simultaneously in a complex circulating fluidized-bed system.

A more general phase diagram, based on the dimensionless groups of Figure 3, is shown in Figure 9 (14). In addition to showing the minimum fluidization velocities and the single-particle terminal velocity, regimes of commercial

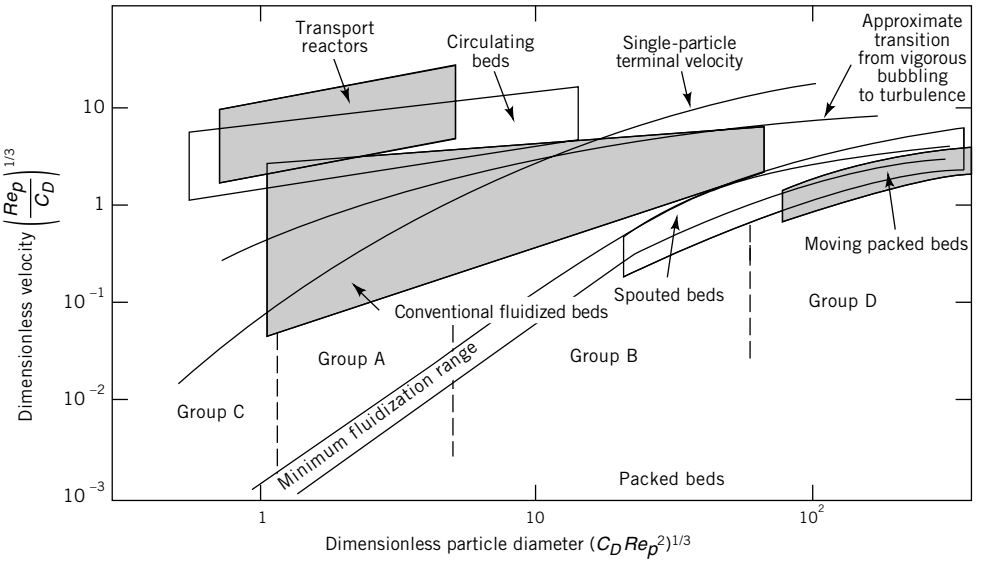

Fig. 9. Nondimensional phase diagram showing Group A, B, C, and D particles (see Fig. 3) (14).

operation are shown for conventional fluidized, ie, vigorously bubbling and turbulent, beds; circulating beds; transport reactors; spouted beds; and moving packed beds. The transition to turbulent fluidization occurs at lower gas velocities for commercial-scale beds than for small-scale beds.

4.1. Pressure Drop. The pressure drop across a two-phase suspension is composed of various terms, such as static head, acceleration, and friction losses for both gas and solids. For most dense fluid-bed applications, outside of entrance or exit regimes where the acceleration pressure drop is appreciable, the pressure drop simply results from the static head of solids. Therefore, the weight of solids in the bed divided by the height of solids gives the apparent density of the fluidized bed, ie,

$$\Delta P/L = \text{suspension density} = \rho_p(1-\epsilon)\left(\frac{g}{g_c}\right) \tag{13}$$

where ϵ is the voidage, the volume fraction of the bed occupied by interparticle gas. The measurement of pressure drop across the bed is the most common and useful diagnostic technique employed for control of fluidized beds.

4.2. Effects of Temperature and Pressure on Minimum Fluidization Velocity. Many basic fluid-bed properties are affected by temperature and pressure. Pressure has little effect on the minimum fluidization velocity, U_{mf}, of fine Group A particles because frictional resistance is mostly a function of viscosity and interparticle forces. However, the larger Group B and D particles show a decrease in minimum fluidization velocity with increasing pressure. The interparticle forces in these groups are usually negligible. The Wen and Yu equation (eq. 11) and the Zenz plot (Fig. 3) both predict this trend. Increasing temperature

increases viscosity and, therefore, reduces U_{mf} for Group A and most Group B particles. The parameter U_{mf} for larger particles is relatively insensitive to temperature, as the effects of increasing viscosity and decreasing density tend to cancel. However, for particle sizes of ~2500 μm and larger, U_{mf} increases with increasing temperature.

4.3. Bubbles and Fluidized Beds. Bubbles, or gas voids, exist in most fluidized beds and their role can be important because of the impact on the rate of exchange of mass or energy between the gas and solids in the bed. Bubbles are formed in fluidized beds from the inherent instability of two-phase systems. They are formed for Group A powders when the gas velocity is sufficient to start breaking interparticle forces at U_{mb}. For Group B powders, where interparticle forces are usually negligible, $U_{mb} = U_{mf}$ and bubbles form immediately upon fluidization. Bubbles, which are inherently undesirable, can grow to a large size in Group B powders and cause contact inefficiencies brought on by significant gas bypassing.

Bubble size control is achieved by controlling particle size distribution or by increasing gas velocity. The data as to whether internal baffles also lower bubble size are contradictory. (Internals are commonly used in fluidized beds for heat exchange, control of solids backmixing, and other purposes.) In some cases, it seems that internals can increase bubble size.

Control of bubble size via particle-size control is easy using Group A powders. A typical Group A powder, having an average particle size of 70 μm and a normal particle size distribution, has nearly 25% of the particles as fines, ie, <44 μm. (Note that FCC catalsyst are usually produced with a lower fraction of fines to minimize particulate losses from FCC regenerator stacks. In such cases, the normal particle size distriubution is truncated to lower the fines concnetration to between 3 and 12%.) If these particles are spherical and if interparticle forces are absent, bubble size is typically <25 mm (see Fig. 5**a**). Well-defined bubbles are not present in the typical industrial turbulent fluidized-bed reactor. The turbulent fluid bed can be viewed as a single-phase system for most practical design considerations. Bubble size control is more difficult for Group B powders, especially in applications where there is little control of particle properties, eg, in processing of naturally occurring materials. In some cases, increasing the gas velocity and moving into turbulent or fast-fluidization regimes has been the preferred solution.

Two-Phase Theory. According to the bubble two-phase theory of fluidization, all gas above that required for minimum fluidization passes through the bed in the form of bubbles. This is only an approximation for Group A particles fluidized at low velocities. Because fluid beds containing Group A solids are usually operated at high multiples of U_{mf}, this two-phase theory has little application in the instance of Group A particles.

Bubbles rise through the bed in two different regimes. Slow bubbles rise at a gas velocity less than V_{mf} (equal to U_{mf}/ϵ_{mf}, and present an opportunity for gas to bypass the bed material and short-circuit through the bubble on the way to the bed surface. Most commercial bubbling fluidized-bed applications have fast-moving bubbles of small size which rise at a gas velocity greater than V_{mf}.

A single bubble rises through a fluid bed at a velocity, U_{br}, proportional to the square root of its diameter, D_b, or more accurately, the diameter of a

sphere of equivalent volume:

$$U_{\mathrm{br}} = 0.71(gD_b)^{0.5} \tag{14}$$

If the bed is slugging, bubble motion is retarded by the bed wall, and the bed or tube diameter, D, rather than the actual bubble diameter, determines the bubble rise velocity, ie,

$$U_{\mathrm{br}} = U_{\mathrm{slug}} = 0.35(gD)^{0.5} \tag{15}$$

The velocity of a bubble in a bubbling bed has been observed to be higher than equation 14 predicts, and it has been suggested that the actual bubble rise velocity in a bubbling bed (15) is

$$U_b = (U - U_{\mathrm{mf}}) + U_{\mathrm{br}} \tag{16}$$

This empirical equation attempts to account for complex bubble coalescence, splitting, irregular shapes, etc. Apparent bubble rise velocity in vigorously bubbling beds of Group A particles is lower than equation 16 predicts.

As bubbles rise through the bed, they coalesce into larger bubbles. The actual bubble size at any height above the distributor, H_{ad}, in the bed is a function of the initial bubble size as it emerges from the gas distributor and the gas flow rate (16):

$$D_b = 0.54(U - U_{\mathrm{mf}})^{0.4}\left[H_{\mathrm{ad}} + 4(A_d/N)^{0.5}\right]^{0.8} \tag{17}$$

where A_d/N is the cross-sectional area of the distributor per distributor hole. For a porous distributor, the distributor area per hole is assumed to be equal to zero. This correlation does not predict the effect of particle-size distribution on bubble diameter.

Bubbles can grow to on the order of a meter in diameter in Group B powders in large beds. The maximum stable bubble size (attained when the rate of bubble coalescence equals the rate of bubble breakup) is limited by the size of the vessel or the stability of the bubble itself. In large fluidized beds, the limit to bubble growth occurs when the roof of the bubble becomes unstable and the bubble splits. Empirically, it has been found that the maximum stable bubble size (D_{bmax}) may be calculated for Group A particles from

$$D_{\mathrm{bmax}} = 2U_t^2/g \tag{18}$$

where U_t is the terminal velocity of a particle 2.7 times the average particle size in the bed. Again, this correlation is only approximate because it contains no information on the most significant factor affecting bubble size, namely particle-size distribution.

4.4. Bed Expansion and Bed Density. Bed density can readily be determined for an operating unit by measuring the pressure differential between two elevations within the bed. This is a highly useful measurement for control and monitoring purposes.

Because bubbles occupy space in a bubbling fluid bed, the expansion of the bed becomes a function of both the bubble velocity and the volume of the gas entering the bed:

$$(H_{max} - H_{mf})/H_{mf} = (U - U_{mf})\,\frac{(U - U_{mf})}{U_{br}} \tag{19}$$

where U_{br} is the single-bubble rise velocity, H_{max} is the operating level of the bed, and H_{mf} is the bed height at minimum fluidization. Extending this volume balance to predict bed densities for bubbling beds gives

$$\rho_{bed} = \rho_{bulk} U_{br}/U_b \tag{20}$$

For turbulent and fast-fluidized beds, bubbles are not present as distinct entities. The following expression for bed voidage, ϵ_{bed}, the volume fraction of the bed occupied by gas, where U is in m/s, has been suggested (17):

$$\epsilon_{bed} = (U + 1)/(U + 2) \tag{21}$$

Bed density can then be predicted from $\rho_{bed} = \rho_p\,(1 - \epsilon_{bed})$. The expression for ρ_{bed} is applicable for turbulent fluidized beds and for the turbulent bottom of fast-fluidized beds fluidized at gas velocities up to 5 m/s.

A more general expression for the expansion of two-phase systems was given in equation 10. It holds for a surprisingly wide range of systems at low and high velocities. This expression can also be used to describe the expansion of gas–solids systems if interparticle forces are negligible. When interparticle forces cannot be neglected, as for Group C and A particles, U_t and n have been shown to depend on the stable cluster size at a given gas velocity (18). The effective U^*_t is then much larger than the single-particle terminal velocity. Bed expansion of a typical Group A powder (FCC catalyst) is shown in Figure 10.

4.5. Solids and Gas Mixing. Solids in an unrestricted fluidized bed can be almost completely backmixed, giving the bed uniform solids properties and a

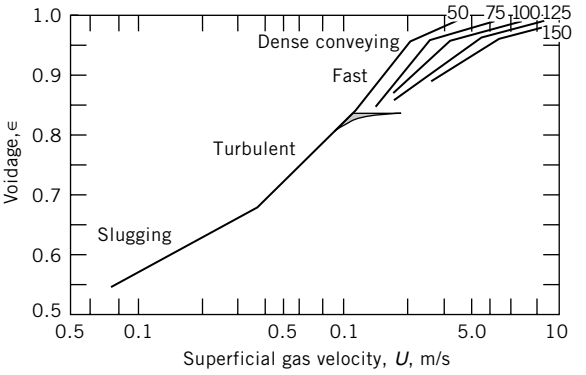

Fig. 10. Expansion curve for FCC catalyst in a 0.15-m inner-diameter column showing the fluidization regimes where the numbers on the lines correspond to the solids rate in kg/(m^2 · s) (18).

constant temperature throughout. The engine driving the solids mixing and circulation is the drag exerted by the gas on the particles. Mixing increases with bed diameter if the bed is not restricted with internals. This increase is linear at first but slows down as the turbulent eddy size is restricted by bed diameter. Beyond a diameter of ~2 m, the eddies no longer grow to the bed diameter, and axial solids (and gas) mixing starts tapering off (19). At small bed diameters the ratio of effective axial dispersion to bed diameter is 1:1; for large diameter beds, this ratio drops to 1:10.

4.6. Mass Transfer. Mass transfer in a fluidized bed can occur in several ways. Bed-to-surface mass transfer is important in plating applications. Transfer from the solid surface to the gas phase is important in drying, sublimation, and desorption processes. Mass transfer can be the limiting step in a chemical reaction system. In most instances, gas from bubbles, gas voids, or the conveying gas reacts with a solid reactant or catalyst. In catalytic systems, the surface area of a catalyst can be enormous. For Group A particles, surface areas of 5 to >1000 m^2/g are possible.

Because particles close to each other are shielded from free gas flow around them, the mass-transfer coefficient for a fluidized-bed system is always less than that for an individual particle in a freely flowing gas. Also, gas entering the bed in a bubble must leave the bubble to react. Interchange with the solid-rich phase occurs mostly by bubble breakage, and more slowly owing to molecular diffusion and gas recirculation from the bubble to the dense phase. The high degree of gas–void splitting in turbulent beds results in a low gas–solids mass-transfer resistance. The section of the fluidized bed near the distributor also shows enhanced mass transfer.

Correlating of mass-transfer data in industrial fluidized beds is most successful when neglecting bubble properties. An example is using an analogy to a staged process where the mass-transfer resistance is related to the height of a diffusion stage. The overall resistance to mass transfer is then the number of diffusion stages or the bed height divided by the individual stage height, ie,

$$N_\alpha = H/H_\alpha \tag{22}$$

where N_α; is the number and H_α; the height of a diffusion stage. For Group A powders in pilot- and commercial-sized units, the height of a stage (20) is

$$H_\alpha = \left(1.8 - 1.06/D^{0.25}\right)\left(3.5 - 2.5/H^{0.25}\right) \tag{23}$$

This equation predicts that the height of a theoretical diffusion stage increases, ie, mass-transfer resistance increases, both with bed height and bed diameter. The diffusion resistance for Group B particles where the maximum stable bubble size and the bed height are critical parameters may also be calculated (21).

4.7. Heat Transfer. One of the reasons fluidized beds have wide application is the excellent heat-transfer characteristics. Particles entering a fluidized bed rapidly reach the bed temperature, and particles within the bed are isothermal in almost all commercial situations. Gas entering the bed reaches the bed temperature quickly. In addition, heat transfer to surfaces for heating and cooling is excellent.

Gas-to-Particle Heat Transfer. Heat transfer between gas and particles is rapid because of the enormous particle surface area available. A Group A particle in a fluidized bed can be considered to have a uniform internal temperature. For Group B particles, particle temperature gradients occur in processes where rapid heat transfer occurs, such as in coal combustion.

In a quiescent fluid, the dimensionless mass-transfer coefficient, or the Nusselt number, $h_{gs}\ d_p/k_f$, for a sphere is two. In fluidized beds the Nusselt number is much less than two for the same reasons given for mass transfer, ie, the particles shield each other from the gas flow.

Bed-to-Surface Heat Transfer. Bed-to-surface heat-transfer coefficients in fluidized beds are high. In a fast-fluidized bed combustor containing mostly Group B limestone particles, the dense bed-to-boiling water heat-transfer coefficient is on the order of 250 W/(m$^2\cdot$K). For an FCC catalyst cooler (Group A particles), this heat-transfer coefficient is around 600 W/(600 m$^2\cdot$K).

The heat-transfer coefficient of most interest is that between the bed and a wall or tube. This heat-transfer coefficient, h, is made up of three components. To obtain the overall dense bed-to-boiling water heat-transfer coefficient, the additional resistances of the tube wall and inside-tube-wall-to-boiling-water must be added. Generally, the conductive heat transfer from particles to the surface, h_{cond}; the convective heat transfer from interstitial gas to the surface, h_{conv}; and the radiative heat transfer, h_{rad}, to the surface are added to give

$$h = h_{cond} + h_{conv} + h_{rad} \tag{24}$$

Radiative heat transfer is negligible if the bed or the heat-transfer surface is $<600^\circ$C.

The heat-transfer coefficient depends on particle size distribution, bed voidage, tube size, etc. Thus a universal correlation to predict heat-transfer coefficients is not available. However, the correlation of Andeen and Glicksman (22) is adequate for approximate predictions:

$$h = \left(900k_f(1-\epsilon)/D\right)\left(GD\rho_s/[\rho_f\mu]\right)\left(\mu^2\Big/\left(d_p^3\rho_s^2 g\right)\right)^{0.326} Pr^{0.3} \tag{25}$$

where Pr is the Prandtl number, $C_p\mu/k_f$.

Fundamental models correctly predict that for Group A particles, the conductive heat transfer is much greater than the convective heat transfer. For Group B and D particles, the gas convective heat transfer predominates as the particle surface area decreases. Figure 11 demonstrates how heat transfer varies with pressure and velocity for the different types of particles (23). As superficial velocity increases, there is a sudden jump in the heat-transfer coefficient as gas velocity exceeds U_{mf} and the bed becomes fluidized.

For Group A solids (Fig. 11**a**) a heat-transfer coefficient of about 900 W/(m$^2\cdot$K) is typical for beds at a fluidized density of 720 kg/m^3 operating in the vigorously bubbling or turbulent fluidization regimes. This coefficient decreases if fines are absent, and decreases as bed density decreases. For Group B solids (Fig. 11**b**) an overall heat-transfer coefficient of 300 W/(m$^2\cdot$K) is typical for beds at a voidage of 0.5 (bubbling fluidized bed). The overall heat-transfer

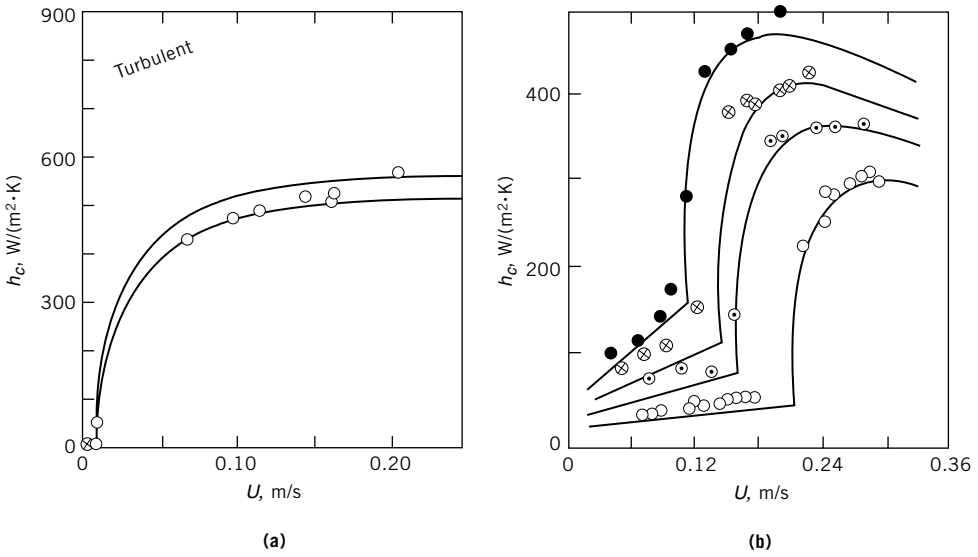

Fig. 11. Variation of heat-transfer coefficient, where ○ represents experimental results at 100 kPa; ⊙, 500 kPa; ⊗, 1000 kPa; and ●, 2000 kPa, of pressure (23) for (**a**) a 0.061-mm glass–CO_2 system (Group A particles) and (**b**) a 0.475-mm glass–N_2 system (Group B and D particles). To convert kPa to psi, multiply by 0.145.

coefficient from the bed to heat-transfer fluid, such as boiling water, inside the tubes is about one-half that value.

5. Distributor Design

Good gas distribution is necessary for the bed to operate properly, and this requires that the pressure drop over the distributor be sufficient to prevent maldistribution arising from pressure fluctuations in the bed. Because gas issues from the distributor at a high velocity, care must also be taken to minimize particle attrition. Many distributor designs are used in fluidized beds. The most common ones are perforated plates, plates with caps, and pipe distributors.

6. Perforated Plates

A perforated plate can be flat, concave, convex, or double dished. The main advantages of the perforated plate are that it is simple, inexpensive, easy to modify, and easy to clean. The disadvantages of a perforated plate are the possibility of solids leaking, ie, weeping through it into the plenum; lower turndown capability than other distributors; the requirement of a peripheral seal; and a relatively high pressure drop required for good distribution.

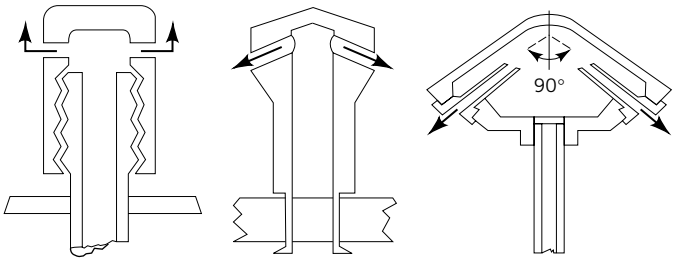

Fig. 12. Cap-type gas distributors where the fluid is directed laterally.

7. Plates with Caps

Several cap-type distributors are shown in Figure 12. These minimize weeping and have good turndown, but are difficult to clean and modify, and are more expensive than perforated plates. A peripheral seal is also required as for a perforated plate.

8. Pipe Distributors

Figure 13 shows two pipe distributors, one in a branched and one in a ring configuration. These distributors minimize weeping, have good turndown, may require the lowest pressure drop, and avoid the need for a plenum chamber. They are also well suited to multiple-level fluid injection. The disadvantages of these distributors are that there are defluidized solids beneath the distributor and the mechanical design is more complex.

8.1. Design Considerations. For a perforated plate, the pressure drop across the distributor should be at least 30% of the bed pressure drop when operating at the lowest expected gas velocity. The number of holes in the distributor should exceed 10/ m^2. The pressure drop, ΔP, across the distributor is given by

$$\Delta P = \frac{\rho}{2}\left(\frac{U_{or}}{C_0}\right)^2 \tag{26}$$

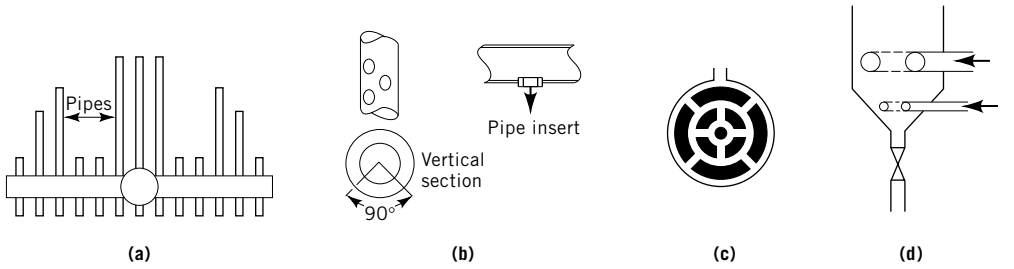

Fig. 13. Examples of pipe gas distributors: (**a**) simple sparger, (**b**) details of the pipe, (**c**) wagon wheel, and (**d**) multilevel distributor.

where the orifice coefficient C_d is usually 0.8, and gas conditions are taken as they exist in the hole and plenum. The space between the holes L_h for a triangular pitch is given as

$$L_h = 1/(N_{\text{or}} \sin 60^\circ)^{0.5} \tag{27}$$

where N_{or} is the hole density (holes per square meter).

In pipe distributors, the pressure drop required for good gas distribution is 30% of the bed pressure drop for upward facing holes, but only 10% for downward facing ones. The pressure drop calculation and the recommended hole density are the same as for a perforated plate. To maintain good gas distribution within the header system, it is recommended the relation

$$\left[D^2_{\text{header}}/\left(ND^2_{\text{or}}\right)\right]^2 > 5 \tag{28}$$

be maintained for good gas distribution, where D_{header} is the pipe header inner diameter and N is the total number of holes in the pipe. The velocity in each header pipe should not exceed 25 m/s, and the holes should be located at least one pipe diameter from a tee or a sharp bend.

8.2. Jet Penetration. At the high gas velocities used in commercial practice, there are jets of gas issuing from distributor holes. It is essential that jets not impinge on any internals, otherwise the internals may be quickly eroded. Figure 14 is a graphical correlation used to determine the jet penetration length as a function of gas velocity and gas density. Jets from horizontal and downflow holes are considerably shorter than those that are pointed upward.

8.3. Particle Attrition. Distributor jets are a potential source of particle attrition. Particles are swept into the jet, accelerated to a high velocity, and smash into other particles as they leave. To reduce attrition at distributors,

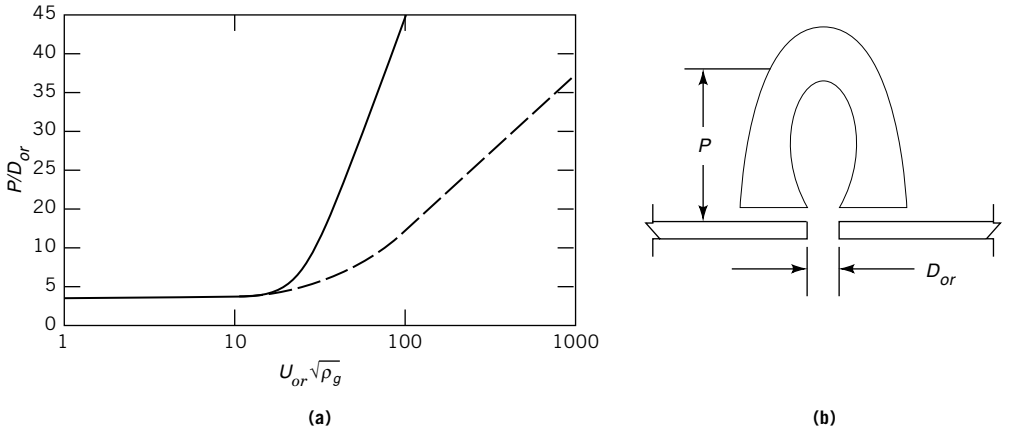

Fig. 14. (**a**) Correlation of jet penetration, P, from distributors into fluidized beds where (—) represents upwardly directed jets and (– – –) downwardly and horizontally directed jets, and U_{or} = throat velocity at point of entry into bed in m/s, and ρ_g = density of gas at nozzle throat in, kg/m^3. (**b**) Schematic defining jet penetration, P, and nozzle or grid hole diameter, D_{or}.

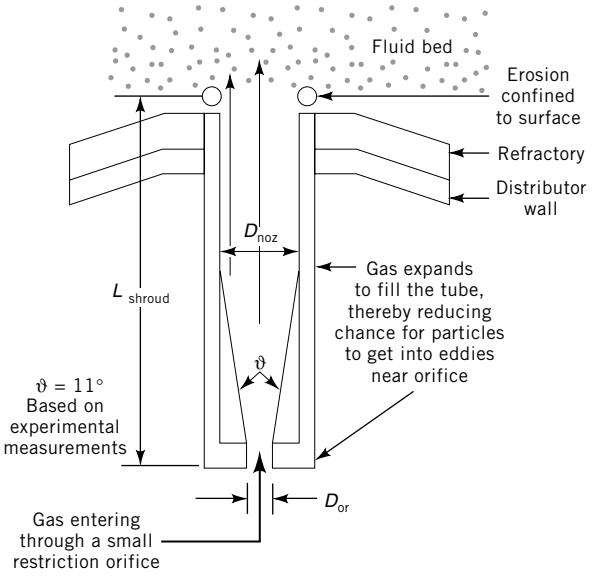

Fig. 15. Schematic of a distributor grid shroud used to allow jets to expand and enter the fluid bed at lower velocity.

a shroud or larger diameter pipe is often added concentric to the jet hole, as shown in Figure 15. The required length of the concentric shroud is given by the relation

$$L_{\text{shroud}} > \cot 5.5^{\circ}\,(D_{\text{noz}} - D_{\text{or}})/2 \tag{29}$$

This shroud length allows the jet issuing from the orifice to expand and fill the shroud. The gas velocity leaving the shroud should not exceed 70 m/s, to minimize attrition.

There are many other potential sources of attrition (24) in a fluidized bed other than high velocity impacts at the distributor. Cyclone inlets and elbows in conveying lines are sources of attrition. Additionally, changes in temperature and chemical reactions can also cause the particles to attrit. A particle's resistance to attrition can be ranked according to its Hardgrove grindability index (HGI), a standard ASTM test (25) originally developed for coal grinding. Special test procedures in ball mills and jet attritors are also common (26).

8.4. Bed Internals. Various types of internals that may be found in commercial fluidized beds include solids and gas distributors; cyclones and cyclone diplegs; solids return and withdrawal lines; heat-transfer tubes; supports, hangers, and guides for heat-transfer tubes; baffles; secondary gas-injection nozzles; and pressure, temperature, and sample probes. Fluidized beds may be completely empty, having only instrumentation tubes penetrating through the vessel walls, or in some cases, they may have significant internals. Heat exchangers can fill a vessel completely and reduce the space between tubes to the minimum required for solids circulation and good maintenance practices.

9. Entrainment

Entrainment, or elutriation, is the carryover of particles from a fluidized bed with the exiting gas. When the gas velocity exceeds the terminal velocity of a Group B particle, the particle is usually removed from the bed. For Group A and C powders, the gas drag needs to overcome interparticle forces as well, and gas velocities of many times the single-particle velocity are needed to entrain particles from the bed at high rates. Knowledge of the entrainment rate is important in order to estimate cyclone inlet loading, solids loss rates, and to predict bed particle size changes resulting from the selective loss of fines.

9.1. Transport Disengaging Height. When the drag and buoyancy forces exerted by the gas on a particle exceed the gravitational and interparticle forces at the surface of the bed, particles are thrown into the freeboard. The ejected particles can be coarser and more numerous than the gas can carry, and some coarse particles and clusters of fines particles fall back into the bed. Some particles also collect near the wall and fall back into the fluidized bed.

The height above the bed at which entrainment becomes essentially constant with height is termed the transport disengaging height (TDH). This is a somewhat arbitrary definition, but it is useful for design. It is desirable to locate cyclones and vessel outlets above TDH so as to minimize solids loading to the cyclones. A schematic drawing illustrating the concept of the TDH is shown in Figure 16. An empirical correlation (4) for estimating the TDH is given in Figure 17 as a function of gas velocity and column size. The estimates are good for TDH at low pressures. However, TDH increases with system pressure (27) and the correlation underestimates TDH at high pressures.

9.2. Entrainment Above TDH. A relatively simple procedure to calculate the amount of entrainment above the TDH is given herein. A more detailed treatment can be found in Ref. 21.

Fine particles in a fluidized bed are analogous to volatile molecules in a boiling solution. Therefore, the concentration of particles in the gas above a fluidized

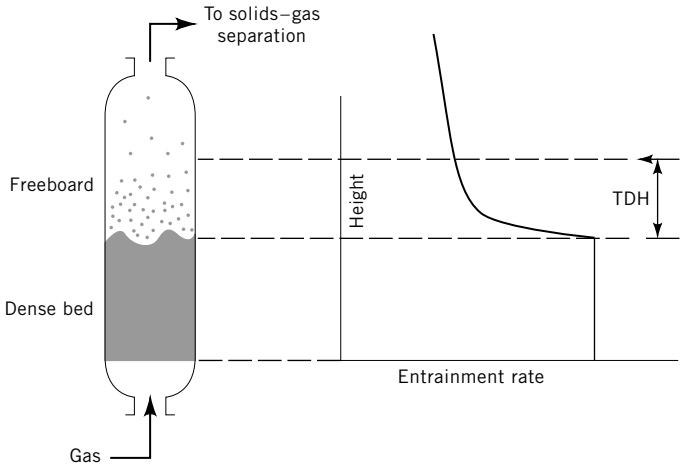

Fig. 16. Transport disengaging height (TDH) (4).

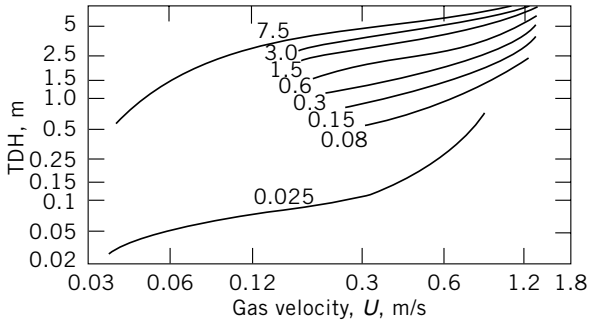

Fig. 17. TDH above vigorously bubbling or turbulent fluidized beds as a function of bed diameter from 0.025 to 7.5 m (28).

bed is a function of the saturation capacity of the gas. To calculate the entrainment rate, it is first necessary to determine what particle sizes in the bed can be entrained. These particles are the ones which have a terminal velocity less than the superficial gas velocity, assuming that interparticle forces in a dilute zone of the freeboard are negligible. An average particle size of the entrainable particles is then calculated. If all particles in the bed are entrainable, the entrained material has the same size distribution as the bed material.

Figure 18 is an entrainment or gas-carrying capacity chart (26). The operating conditions and particle properties determine the vertical axis; the entrainment is read off the dimensionless horizontal axis. For entrainment purposes, the particle density effect is considered through the ratio of the particle density to the density of water. When the entrainable particle-size distribution is smaller than the particle-size distribution of the bed, the entrainment is reduced by the fraction entrainable, ie, the calculated entrainment rate from Figure 18 is multiplied by the weight fraction entrainable.

In practice, the entrained material is enriched in fines even when the entire bed is entrainable. However, as the gas velocity is increased to many multiples of the terminal velocity, the composition of the entrainable material approaches the bed composition.

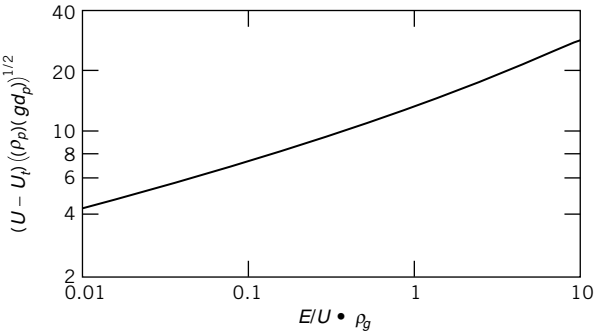

Fig. 18. Correlation of entrainment rate and composition (28).

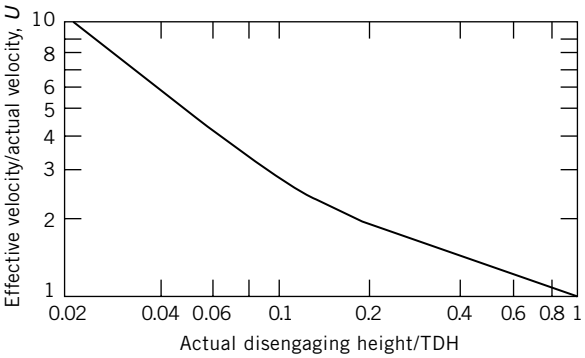

Fig. 19. Effective velocity for entrainment below TDH (28).

Normally vessels are designed with the gas outlet location well above TDH. If circumstances force operation with a bed height so that the outlet is below TDH, an equivalent velocity, an effective velocity higher than the actual superficial gas velocity, is used in the above calculation. The effective gas velocity can be determined from Figure 19 (28).

9.3. Cyclones. Cyclones are an integral part of most fluidized-bed systems. A cyclone is an inexpensive device having no moving parts that separates solids and gases using centrifugal force. A basic cyclone is shown in Figure 20.

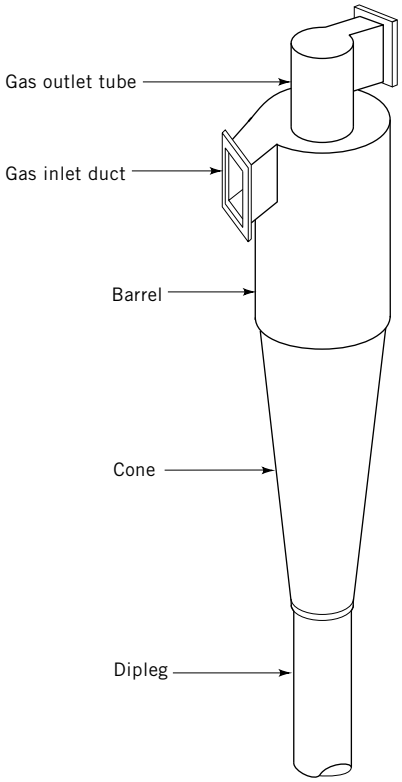

Fig. 20. The basic cyclone.

The solid–gas mixture enters the cyclone tangentially through a rectangular duct. The gas velocity and the curvature of the cyclone body combine to subject the particles to a centrifugal force up to 100 times gravity. The particles are forced to the wall, spiral to the bottom, and the solids-free gas exits through the center outlet tube at the top of the cyclone. Cyclones are used commercially to remove solids with high efficiency down to ~15 μm. Other aspects of cyclone design may be found in Refs. 28 and 29. (see also AIR POLLUTION CONTROL METHODS).

10. Circulating Fluidized Beds

Circulating fluidized beds (CFBs) are high velocity fluidized beds operating well above the terminal velocity of all the particles or clusters of particles. A very large cyclone and seal leg return system are needed to recycle solids in order to maintain a bed inventory. There is a gradual transition from turbulent fluidization to a truly circulating, or fast-fluidized bed, as the gas velocity is increased (Fig. 6), and the exact transition point is rather arbitrary. The solids are returned to the bed through a conduit called a standpipe. The return of the solids can be controlled by either a mechanical or a nonmechanical valve.

The bed level is not well defined in a circulating fluidized bed, and bed density usually declines with height. Axial density profiles for different CFB operating regimes show that the vessel does not necessarily contain clearly defined bed and freeboard regimes. The solids may occupy only between 5 and 20% of the total bed volume.

10.1. Pressure Balance and Standpipes. The pressure balance around the loop of a circulating fluidized bed is illustrated in Figure 21. The driving force of a high gas velocity entering the bed expands the bed volume and carries solids out of the bed. The pressure drop is lower than in a dense fluidized-bed system, because the solids occupy a smaller fraction of the volume. Another pressure drop exists across the cyclone system. The solids flow from the cyclone into a standpipe that returns them to the bottom of the bed. Pressure builds up in the standpipe to allow the solids to flow back into the high pressure zone at the bottom of the CFB. The maximal pressure buildup in the standpipe is obtained by keeping the solids in the standpipe fluidized. The fluidized solids in the standpipe develop a pressure head like any fluid. Some of this pressure buildup can then be dissipated across a control valve to regulate solids flow and form a seal against gas flow back into the standpipe.

Whereas standpipes have been in operation for many years, many aspects of their operation are not well understood. The purpose of a standpipe is to transfer solids from a region of low pressure to a region of higher pressure. In a properly operating standpipe of Group A solids, the solids are moving downward at a relative gas–solids velocity $>U_{mf}/\epsilon$. The relative gas solids velocity, V_r, is defined as

$$V_r = V_s - U/\epsilon \tag{30}$$

This causes the solids to be fluidized. In practice, the solids are moving so fast that interstitial gas and gas bubbles are dragged downward with them.

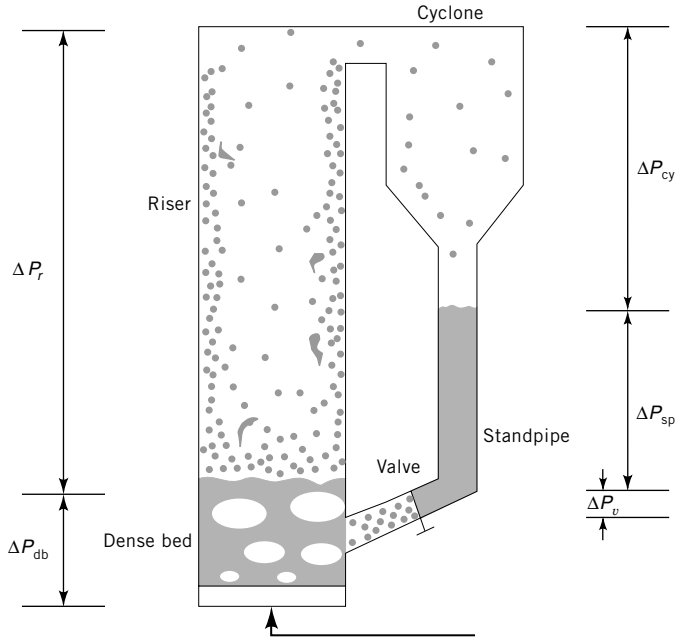

Fig. 21. CFB pressure balance, where $\Delta P_{sp} = \Delta P_v + \Delta P_{db} + \Delta P_r + \Delta P_{cy}$. A high gas velocity in a fast bed results in a high solids entrainment rate. Head buildup in the standpipe overcomes head buildup in the dense bed, riser, cyclone, and sealing device (valve), and allows solids to recirculate.

The gas volume dragged down the standpipe is compressed owing to the pressure buildup, and may cause the solids to become defluidized. Figure 22 shows that the pressure buildup in a standpipe can be reduced, or even become negative. Aeration can be added to the standpipe to prevent the gas volume reduction causing defluidization because of the pressure increase. The suggested amount of aeration to add to the standpipe to overcome the effects of gas

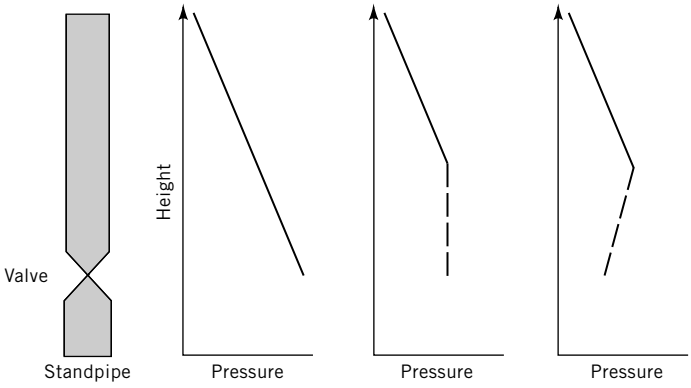

Fig. 22. Standpipe and standpipe pressure profiles showing (—) fluidized flow and (– – –) packed bed or defluidized flow.

compression may be calculated from the following expression:

$$Q_{\min} = \left[\frac{P_b}{P_t}\left(\frac{1}{\rho_{\mathrm{mf}}} - \frac{1}{\rho_s}\right) - \left(\frac{1}{\rho_t} - \frac{1}{\rho_s}\right)\right] \tag{31}$$

Note that the solids density used in this equation should be the true solids, ie, skeletal, density, because the gas in the pores is also compressed. For Group A solids the aeration gas should also be added evenly along the standpipe.

Group B solids have higher minimum fluidization velocities than Group A solids. For best results for Group B solids flowing in standpipes, standpipe aeration should be added at the bottom of the standpipe, not uniformly along the standpipe (R) (30).

10.2. Nonmechanical Valves. Nonmechanical valves, which have no moving parts in the solids flow path, are often used to control the flow of Group B solids. Examples of nonmechanical valves are an L-valve, J-valve, loop seal, and reverse seal. A nonmechanical L-valve joins a pneumatic conveying line or a fluidized bed in the shape of a capital L. The elbow of the L-valve does not allow solids to flow unless aeration is added in the vertical part of the L-valve. The optimum location for aeration is approximately one pipe diameter above the horizontal centerline. The amount of solids flow is a function of the amount of aeration added to the L-valve (31). This system can operate under hot, corrosive, and erosive environments which would be too difficult for mechanical valves. L-valves also cost significantly less than mechanical valves. L-valves work best with Group B powders. Nonmechanical valves have also been used for many years in moving beds of Group D particles, such as in the Thermofor catalytic cracker (TCC).

11. Scale Up of Fluidized Beds

The greatest problems in scaling up fluidized beds have been encountered using Group B solids where bubbles can grow to very large sizes and bubble size control is more difficult than with Group A solids. A pilot-plant or laboratory-scale fluidized bed can operate where bubbles are no more than several centimeters in diameter because of the limiting small diameter of the bed (see PILOT PLANTS AND MICROPLANTS). However, a larger commercial unit can have bubbles up to one meter in diameter. The larger bubbles flow through the bed at a high velocity, and the gas inside the bubble has little interaction with the solids.

Several attempts have been made to determine proper scaling relationships for Group B fluidized beds. These early attempts, and a rigorous derivation by nondimensionalizing the basic differential equations governing fluid and solids flow, have been summarized (32). The basic scaling factors are Reynolds number (eq. 5); Froude number where

$$\text{Froude number} = \frac{U^2}{gd_p} \tag{32}$$

density ratio, ρ_p/ρ_g; length ratios, L/d_p and D/d_p; and other factors such as ψ, sphericity, particle size distribution, and bed geometry.

There are some data to suggest that hydrodynamic similarity improves scale-up for two-phase systems such as fluidized beds, even though it is not as convincing as single-phase evidence. To use these scaling factors to simulate large-scale hot systems, small-scale cold flow testing needs to hold the ratios of several variables constant. For example, to scale from a cold (15°C) to a large, hot (800°C) system, the following ratios are recommended (32):

Variable	Ratio
velocity, U	0.5
particle size, d_p	0.25
particle density, ρ_p	3.5
bed height, H	0.25
bed diameter, D	0.25

This scaling method has several limitations. There has been concern about changing particle properties for complex, wide distributions of naturally occurring materials. This analysis ignores interparticle forces, and hence does not apply to Group C and A powders.. Moreover, this analysis is too simplistic to take into consideration rapidly changing conditions, such as occur near a distributor region in a fluidized bed.

Group A particles cause fewer scale-up problems because fluidized beds of Group A particles generally are operated in the vigorously bubbling or turbulent fluidization regimes. Also, it is not unusual for a maximum stable bubble—gas void to be on the order of 25 mm or less for these particles. Thus a pilot-plant facility can generally be operated using the same gas void size that a commercial unit would experience. An example of scale-up concerns and ways to avoid them for Group A powders is shown in Figure 23 (33). In this case, the efficiency was

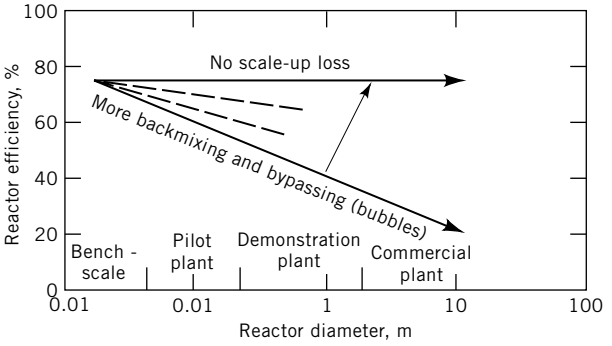

Fig. 23. Turbulent and bubbling beds scale-up comparison where increasing gas velocity, fines content, and H/D staging can help maintain reactor efficiency as the reactor diameter increases. A 100% efficiency is equivalent to plug flow.

maintained at 80% for a turbulent fluidized bed, ie, there was no scale-up loss, but efficiency decreased with scale up for a bubbling bed. Adding fines and operating at a higher gas velocity in a bubbling bed, ie, moving it toward turbulence, can offset scale-up loss.

Bubble size is controlled by maintaining the content of fines in a catalyst blend at a concentration of between 15 and 30%. This helps to keep gas voids unstable and small, and minimizes gas bypassing via the gas voids in the bed. Using a high gas velocity also helps to approximate plug flow of the gas. To minimize scale-up problems using Group A solids, the bed should be operated in the turbulent regime, which requires a gas velocity of 0.5 to 1 m/s. Bed internals can be beneficial in reducing solids backmixing, which can lower the efficiency of most reactions. Because of inherent backmixing, the best fluidized-bed reactor has an efficiency equivalent to approximately 80% of a plug-flow reactor.

Some backmixing is important to ensure temperature uniformity, but excessive backmixing can lead to high axial dispersions and hence rapid decrease in performance (Fig. 23). Bed internals, a combination of vertical heat-exchange tubes and horizontal baffles and hangers, are used in many Group A catalytic reactors such as those for acrylonitrile, ethylene dichloride, etc, to eliminate scale-up losses. Scale up for such reactions using Group A powders is simple as long as basic sound design principles are used. Successful scale ups of such reactions from 25-mm inner-diameter pilot plants to 10-m diameter commercial units have been achieved in one step, as was the case for acrylonitrile in the 1950s. The design principles of a commercial turbulent fluidized-bed reactor of Group A powders are illustrated schematically in Figure 24. The key variables that ensure successful and simple scale up are particle properties (sufficient fines); gas velocity in the turbulent fluidization regime; proper distributor design; internals, with appropriate open area; and primary cyclone diplegs which return the entrained fines to the region where they are needed most for bubble size control, ie, near the distributor. Using these principles, scale up of Group A catalytic fluidized-bed reactors can be easily accomplished.

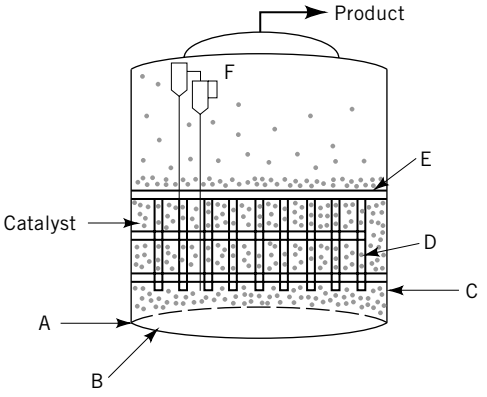

Fig. 24. Elements of a bubbleless turbulent fluid-bed reactor design where the internals create four stages. A represents the shrouded grid; B, the first feed; C, the second feed; D, heat exchange; E, staging; and F, the cyclones and/or filters.

12. Use of Computational Fluid Dynamics

It is possible to describe fluid-bed behavior based on first principles derived from the Navier-Stokes equations. There are two approaches to doing these calculations. The first is to keep track of the behavior of each particle in the system and this is called a Lagrangian based model. Because each particle is accounted for, the calculation is generally done for several thousand large particles usually of the same size. Uncertainties associated with the calculation are such things as

- Coefficient of restitution of the particles.
- Wall friction.
- Turbulence terms for the fluid and how the turbulence is affected by particles.
- Absence of many finer particles that are usually present in real systems.

The second method of calculation is called Eulerian. In this simulation, the particles and their immediate surrounding fluid are treated as a pseudo-fluid through which gas is flowing. This method has the advantage of applying to catalyst sized particles. Again, a number of assumptions are required for the calculation and uncertainties are present.

- "Viscosity" of the pseudo-fluid.
- Wall friction terms.
- Turbulence factors.
- Particle size effects.
- Pseudo-fluid gas friction terms.

The use of CFD has shown promise in fitting observed fluid bed behaviors (Gidaspow or Sinclair in Circ Fluid Beds). However, a recent test problem worked on by several modelers yielded mixed results for predicting the observed behaviors. (Knowlton). CFD is used today in major companies as a decision aid to understand general trends but is not yet considered a design tool. However, the steadily increasing computational power available to CFD should bring about improvement in its accuracy as a predictive tool for fluid bed systems.

An interesting review of contacting efficiency of various types of fluidized beds is given by Kunii and Levenspiel (34).

13. Nomenclature

A	area of bed
A_d	cross-sectional area of distributor
Ar	Archimedes number, $\rho_g d_p^3(\rho_p - \rho_g)g/\mu^2$
C_d	drag coefficient
D	bed diameter
D_b	diameter of bubble

D_{bmax}	maximum stable bubble diameter
D_{noz}	diameter of nozzle
D_{or}	diameter of orifice
D_{header}	diameter of pipe header
d_p	"average" particle diameter
d_{pw}	weight average particle diameter
d_{pi}	particle diameter of an individual cut
d_{sv}	surface mean particle diameter
d_v	volume average diameter
E	entrainment rate ($kg/s \cdot m^2$)
G	solids mass flux
g	gravitational acceleration
g_c	conversion factor (in SI units $g_c = 1$)
H	height of fluidized bed
H_{ad}	height above distributor
H_α	height of a diffusion stage
H_{max}	maximum bed height
H_{mf}	bed height at minimum fluidization
h	heat-transfer coefficient from a fluidized bed to a heat-transfer surface
h_{cond}	conductive heat-transfer coefficient
h_{conv}	convective heat-transfer coefficient
h_{gs}	gas–solids heat-transfer coefficient
h_{rad}	radiative heat-transfer coefficient
k_f	thermal conductivity of gas
L	length
L_h	distributor pitch
L_{shroud}	length of shroud
n	Richardson-Zaki coefficient
N	number of distributor holes
N_a	number of diffusion stages
N_{or}	distributor hole density
P	jet penetration length
P_b	absolute pressure at bottom of standpipe
Pr	Prandtl number, $C_p\mu/K$
P_t	absolute pressure at top of standpipe
Q	gas volumetric flow rate
Q_{bubble}	volume flow rate of bubbles
Q_{mf}	gas volumetric flow rate at minimum fluidization
Q_{min}	minimum aeration required to maintain fluidized conditions in a standpipe, actual cubic meters per second of aeration required (at standpipe conditions) per kg of solids flowing down the standpipe
Re_p	particle Reynolds number, $d_p U \rho_g/\mu$
TDH	transport disengaging height
U	superficial gas velocity
U_b	bubble rise velocity in a bubbling bed
U_{br}	single bubble rise velocity
U_{mb}	minimum bubbling velocity
U_{mf}	minimum fluidization velocity
U_{or}	gas velocity through an orifice in a distributor
U_{slip}	gas–solids velocity
U_{slug}	riser velocity of slug
U_t	single-particle terminal velocity
U_t^*	effective or "cluster" terminal velocity
V_{mf}	interstitial minimum fluidization velocity, U_{mf}/ϵ_{mf}
V_r	relative gas–solids velocity
V_s	solids velocity
X_i	weight fraction
Δ	characteristic system length

ΔP	pressure drop
ΔP_{cy}	cyclone pressure drop
ΔP_{db}	dense bed pressure drop
ΔP_r	riser pressure drop
ΔP_{sp}	standpipe head buildup
ΔP_v	valve pressure drop
ϵ	gas voidage (volume fraction occupied by gas)
ϵ_{bed}	voidage in bed
ϵ_{mf}	voidage at minimum fluidization
μ	gas viscosity
ρ_{bulk}	bulk density of solids
ρ_{mf}	bed density at minimum fluidization
ρ_g	gas density
ρ_p	solids density
ρ_s	true solids (skeletal) density
ρ_t	fluidized density at top of standpipe
	particle sphericity

BIBLIOGRAPHY

"Fluidization" in *ECT* 1st ed., Suppl. 1, pp. 365–400, by F. A. Zenz, Consultant; in *ECT* 2nd ed., Vol. 9, pp. 398–445, by F. A. Zenz, Consultant; in *ECT* 3rd ed., Vol. 10, pp. 548–581, by F. A. Zenz, Consultant; in *ECT* 4th ed., Vol. 11, pp. 138–171, by A. A. Avidan, Bechtel Corporation, D. F. King, Chevron Texaco, T. M. Knowlton, Institute of Gas Technology/Particulate Solids Research Inc., M. Pell, E. I. du Pont de Nemours & Co., Inc.; "Fluidization" in *ECT* (online), posting date: December 4, 2000, by Amos A. Avidan, Mobil Research and Development Corporation, Desmond F. King, Chevron Research and Technology Company, Ted M. Knowlton, Institute of Gas Technology/Particulate Solids Research Inc., Mel Pell, E. I. du Pont de Nemours & Co., Inc.

CITED PUBLICATIONS

1. D. Geldart, ed., *Gas Fluidization Technology*, John Wiley & Sons, Inc., Chichester, U.K., 1986.
2. A. A. Avidan, M. Edwards, and H. Owen, *O G J.*, 33 (Jan. 8, 1990).
3. J. F. Richardson and W. N. Zaki, *Trans. Inst. Chem. Eng.* **32**, 35 (1954).
4. F. A. Zenz and D. F. Othmer, *Fluidization and Fluid Particle Systems*, Reinhold Publishing Corp., New York, 1960.
5. C. Y. Wen and Y. H. Yu, *AIChE J.* **12** 610, (1966).
6. D. Geldart, *Powder Technol.* **7**, 285 (1973).
7. J. M. Matsen, *AIChE Symp. Ser.* **69**, 30 (1973).
8. D. Geldart and H. Y. Xie, in O. E. Potter and D. J. Wicklin, eds., *Fluidization VII Proceedings*, Engineering Foundation, New York, 1992, pp. 749–756.
9. R. J. de Vries, W. P. M. van Swaaij, C. Mantovan, and A. Heijkoop, *Chem. React. Eng. Proc. Eur. Symp.* **5**, **B9** (1972).
10. A. M. Squires, M. Kwauk, and A. A. Avidan, *Science* **230**(4732), 1329 (1988).
11. K. Rietema, *The Dynamics of Fine Powders*, Elsevier Applied Science Publishers Ltd., London, 1991.

12. J. Yerushalmi and A. A. Avidan, in J. F. Davidson, R. Clift, and D. Harrison, eds., *Fluidization*, 2nd ed. Academic Press, London, 1985.
13. J. Yerushalmi, N. T. Cankurt, D. Geldart, and B. Liss, *AIChE Symp. Ser.* **74**(176), 1–13 (1978).
14. J. R. Grace, *Can. J. Chem. Eng.* **64**, 353 (June 1986).
15. J. F. Davidson and D. Harrison, *Fluidised Particles*, Cambridge University Press, Cambridge, U.K., 1963.
16. R. C. Darton, R. D. LaNauze, J. F. Davidson, and D. Harrison, *Trans. Inst. Chem. Eng.* **55**, 274 (1977).
17. D. F. King, D. F. King, in *Fluidization VI Conference*, Engineering Foundation, New York, 1989, pp. 1–8.
18. A. A. Avidan, *Bed Expansion and Solids Mining in High-Velocity Fluidized Beds*, Ph.D. dissertation, City University of New York, 1980.
19. A. A. Avidan and J. Yerushalmi, *AIChE J.* **31**(5), 835 (1985).
20. W. P. M. van Swaaij, and F. J. Zuiderweg, in H. Angelino, ed., *Proceedings of the International Symposium on Fluidization and its Applications*, Cepadues-edit, Toulouse, France, 1973, pp. 454–467.
21. M. Pell, *Gas Fluidization*, Elsevier, Amsterdam, The Netherlands, 1990.
22. B. R. Andeen and L. R. Glicksman, ASME/AIChE Heat Transfer Conference, St. Louis, Mo., 1976, paper 76HT-67.
23. D. F. King, *Fluidization Under Pressure*, Ph.D. dissertation, University of Cambridge, U.K., 1979.
24. J. Werther and J. Reppenhagen, *AIChE J.* **45** (2001).
25. ASTM D409-85 *1988 Annual Book of ASTM Standards*, 05.05, American Society for Testing and Materials, Philadelphia, Pa., 1988, pp. 186–190.
26. J. E. Gwyn, *AIChE J.* **15**, 35 (1969).
27. I. Chan and T. M. Knowlton, *AIChE Symp. Ser.* No. 241, Vol. **80**, 24 (1984).
28. *Manual of Disposal of Refinery Wastes*, Volume on Atmospheric Emissions, API Publication 931, American Petroleum Institute, Washington, D.C., May 1975, "Chapt. 11."
29. A. C. Hoffman, L. E. Stein, *Gas Cyclones and Swirl Tubes*, Springer-Verlag, Berlin, 2002.
30. T. M. Knowlton in Wen-Cheng Yang, ed., *Handbook of Fluidization and Fluid-Particle Systems*, Marcel Dekker, Inc., New York, 2003, Chapt. 21, p. 580.
31. T. M. Knowlton and I. Hirsan, *Hydrocarbon Process.* **57**, 149 (1978).
32. L. R. Glicksman, *Chem. Eng. Sci.* **39**(9), 1373 (1984).
33. A. A. Avidan and M. Edwards, in K. Østergaard and A. Sørensen, eds., *Fluidization V Conference*, Engineering Foundation, New York, 1986, pp. 457–464.
34. D. Kunii and O. Levenspiel, *Chem. Eng. Sci.* **52**(15), 2471 (1997).

AMOS A. AVIDAN
Bechtel Corporation

DESMOND F. KING
Chevron Texaco

TED M. KNOWLTON
Institute of Gas Technology/
Particulate Solids Research Inc.

MEL PELL
E. I. du Pont de Nemours & Co., Inc.